Interphase Drag Coefficients in Gas–Solid Flows

D. Kandhai, J. J. Derksen, and H. E. A. Van den Akker
Kramers Laboratorium voor Fysische Technologie, Faculty of Applied Sciences, Delft University of Technology, Prins Bernhardlaan 6 2628 BW Delft, The Netherlands

Gas–solid fluidized-bed reactors are commonly used in the process industries due to their high operational efficiency regarding, for instance, solids mixing and heat and mass transfer (Geldart, 1986). It is well known that hydrodynamics plays a crucial role in the dynamic behavior of fluidized beds (Geldart, 1986; Fan and Zhu, 1998). Currently, computational fluid dynamics methods are widely used to obtain a better understanding of the complex behavior due to gas–solid (hydrodynamic) and solid–solid (collisional) interactions and, of course, how this emergent behavior affects the operation of fluidized-bed reactors (see, for example, Goldschmidt et al., 2000).

Numerical simulations of fluid dynamics in such systems are generally based on the so-called two-fluid models (Fan and Zhu, 1998). In these models, both phases are considered as interpenetrating continua. Mass, momentum, and (in some cases) energy balances are derived using volume and time or ensemble averaging techniques. For example, the momentum equations for the gas phase in the case of isothermal flow follow the relation

$$\frac{\partial}{\partial t}(\epsilon\rho_g \boldsymbol{u}) + (\nabla\cdot\epsilon\rho_g \boldsymbol{u}\boldsymbol{u}) = -\epsilon\nabla p - \beta(\boldsymbol{u}-\boldsymbol{v}) - \nabla\cdot(\epsilon\boldsymbol{\Pi}) + \epsilon\rho_g \boldsymbol{g} \quad (1)$$

Here $\boldsymbol{u}$ and $\boldsymbol{v}$ are the velocity of the gas and solid phase, respectively; ϵ is the gas volume fraction; ρ_g is the density of the gase; p is the pressure; $\boldsymbol{\Pi}$ is the stress tensor; g is the gravitational acceleration, and β is the interphase drag coefficient, which is the primary subject of this study. This β term is a closure relation for the drag force exerted on the solid particles by the gas phase, as a function of the solid volume fraction, $\phi = 1-\epsilon$, and the particle Reynolds number, $Re = (\epsilon|\boldsymbol{u}-\boldsymbol{v}|2a)/\nu$ (with a the radius of the spherical solid particles and ν the kinematic viscosity of the gas phase).

In many cases, the well-known Wen and Yu (1966) and the Ergun (1952) equations are used to describe interphase drag coefficients. The Ergun correlation expressed in terms of the nondimensional drag force acting on a single particle, F, is given by

$$F = 8.33\frac{\phi}{(1-\phi)^3} + \frac{0.18}{2}\frac{Re}{(1-\phi)^3} \quad (2)$$

Here F is made dimensionless by the gas-volume fraction, ϵ, and the Stokes drag acting on a single sphere in an infinite medium, $F_s = 6\pi\rho_g \nu a \epsilon|\boldsymbol{u}-\boldsymbol{v}|$.

The Wen and Yu (1966) correlation follows the relation

$$F = (1+0.15Re^{0.687})(1-\phi)^{-4.65} \quad (3)$$

Notice that F is related to β through the expression $F = \beta \times (2a)^2/(18\epsilon^2(1-\epsilon)\rho_g \nu)$.

The Wen and Yu correlation, a refinement of the Richardson and Zaki equation (1954), is based on particle fluidization experiments performed in a wide range of solid-volume fractions and Reynolds numbers, $0.4 < \phi < 1.0$ and $0.01 < Re < 5{,}000$, respectively. The Ergun equation, on the other hand, is derived from pressure-drop measurements in closed-packed fixed beds. Furthermore, although the latter is based on systems with particles on fixed positions, it can be applied to dynamic systems, as well, if the density ratio between the two phases (as generally is the case in gas–solid flow) is large (Koch, 1990).

In numerical simulations of gas–solid fluidized-beds, it is still unclear which correlation should be used for describing the interphase drag coefficients. The two widely used models are the Wen and Yu equation and a hybrid model, suggested by Gidaspow (1994), with Wen and Yu for $\phi < 0.2$ and Ergun otherwise. In a recent study, it has been shown by van Wachem et al. (2001) that the exact choice of the closure relation can have a significant influence on, for example, the simulated bubble shapes in fluidized beds.

Correspondence concerning this article should be addressed to D. Kandhai.

Recently, Hill et al. (2001) performed a rigorous study concerning the dependence of the drag force on Re and ϕ for a wide range of solid-volume fractions. By using a lattice–Boltzmann method, the drag force acting on fixed (dis)ordered monodisperse bead packings in periodic domains was computed. For dense systems ($\phi \geq 0.5$), the simulated drag curve is in good agreement with the Ergun equation, in contrast to that in the less dense regime. However, a connection with the Wen and Yu equations was not reported, leaving the following question unresolved: Which ϕ should one differentiate between the dilute and dense regimes?

In this article, we revisit the drag-force closures problem and focus on the question: Is the hybrid model indeed valid, or should we instead discriminate between a dilute, dense, and an intermediate regime? For this we perform lattice–Boltzmann (Chen and Doolen, 1998) simulations of fluid flow in fixed monodisperse disordered periodic sphere packings in the range $1 < Re < 50$ and $0.1 < \phi < 0.5$, and compare our results with that obtained by Hill et al. (2001) and with the Wen and Yu and the Ergun correlations.

Simulation Method

In simulations, we consider fluid flow through disordered arrays of spheres in a periodic box. For the computation of the flow fields and the drag force, we use the lattice–Boltzmann method (LBM). In the past decade, LBMs have proven to be versatile tools in simulating a wide variety of applications, ranging from creeping flow in porous media (Kandhai et al., 2002a,b) to turbulent flows in stirred-tank reactors (Derksen, 1999). These methods originated from the lattice gas automata (LGA), which are discrete models for the simulation of transport phenomena. In LGA, fictitious particles move synchronously along the bonds of a regular lattice and interact locally according to a given set of rules subject to conservation of mass and momentum. Due to this inherent spatial and temporal locality, these methods are well suited for parallel computing. In contrast to LGA, in LBM a density of particles is being tracked rather than a single one, and there is relatively more freedom in the formulation of the collision operator (Chen and Doolen, 1998). The simplest collision model is the Bhatnagar–Gross–Krook (BGK) scheme with a single time relaxation to the local equilibrium distribution. The corresponding lattice–BGK method (Chen and Doolen, 1998) is given by

$$f_i(\boldsymbol{r}+\boldsymbol{c}_i,t+1) = f_i(\boldsymbol{r},t) + \frac{1}{\tau}\left[f_i^{(0)}(\boldsymbol{r},t) - f_i(\boldsymbol{r},t)\right] \quad (4)$$

where $\boldsymbol{c}_i$ is the ith link; $f_i(\boldsymbol{r},t)$ is the density of particles moving in the $\boldsymbol{c}_i$-direction; τ is the BGK relaxation parameter; and $f_i^0(\boldsymbol{r},t)$ is the equilibrium distribution function toward which the particle populations are relaxed. A common choice for $f_i^0(\boldsymbol{r},t)$ is,

$$f_i^0 = t_i\,\rho\left[1 + \frac{1}{c_s^2}(\boldsymbol{c}_i\cdot\boldsymbol{u}) + \frac{1}{2c_s^4}(\boldsymbol{c}_i\cdot\boldsymbol{u})^2 - \frac{1}{2c_s^2}u^2\right] \quad (5)$$

where t_i is a weight-factor, which depends on the length of the vector $\boldsymbol{c}_i$; c_s is the speed of sound; and ρ is the density. The density and the velocity are obtained from moments of the discrete velocity distribution $f_i(\boldsymbol{r},t)$

$$\rho(\boldsymbol{r},t) = \sum_{i=0}^{N} f_i(\boldsymbol{r},t) \quad \text{and} \quad \boldsymbol{u}(\boldsymbol{r},t) = \frac{\sum_{i=0}^{N} f_i(\boldsymbol{r},t)\boldsymbol{c}_i}{\rho(\boldsymbol{r},t)} \quad (6)$$

with N denoting the number of links per lattice point. The kinematic viscosity ν in lattice units (l.u.) is given by $\nu = (\tau - 1/2)/3$. For our current purpose, we use the so-called D_3Q_{19} lattice–BGK model (Chen and Doolen, 1998).

In the simulations, the flow is driven by a body force, that is, at each time step a fixed amount of momentum is added to all lattice points. The solid–fluid interface is modeled by using the well-known bounce-back method, that is, particles entering a solid node are reflected to the fluid with reversed velocity. Steady state in the simulation is achieved when the total body force acting on the fluid is equal to the drag force exerted on the solid matrix. The Reynolds number is now varied by adjusting the body force.

Results and Discussion

Generally, the computational grid in LB simulations is uniform and Cartesian. Extension of the method to irregular grids is available, although its application is still restricted to single-particle systems due to limited computational resources (Rohde et al., 2002). As a consequence, the discrete representation of a sphere in disordered arrays is staircased. The staircasing of the surface, the way solid–fluid boundaries are imposed and the actual accuracy of the method, are reflected in the discretization error (Kandhai et al., 1999). From preliminary finite-size studies, we conclude that, for the low solid fractions, a sphere discretization with a diameter of 10 lattice points yields satisfactory results, that is, discretization errors are then around 10%. For the denser systems, known to be much more sensitive to numerical errors due to the limited number of channels through which the fluid can percolate, we have to discretize the spheres with a diameter of some 20 lattice points to obtain similar accuracies (see Figure 1).

In LBM schemes, yet another artifact exists, namely, a dependence on the fluid viscosity of the radius of particle that is actually being simulated (the so-called hydrodynamic radius). One way to correct for this effect is by applying the following procedure (Ladd, 1994):

- First, the hydrodynamic radius corresponding to a certain geometrical radius and kinematic viscosity is computed by using the analytical solution of creeping flow through a periodic array of spheres (in the dilute limit) (Hasimoto, 1959).
- Next, the many-particle computations are calibrated by taking the hydrodynamic radius as the true radius of the particles.

The corresponding hydrodynamic radii of spheres in a fluid flow with kinematic viscosity of 0.067 (in l.u.) and discretized using 10 and 20 lattice points, are 10.4 and 20.4, respectively (in l.u.). In Figure 2, we show the results obtained for the drag force as a function of the Reynolds number for $\phi \approx 0.3$ (after calibration). It is clear, that after having applied the

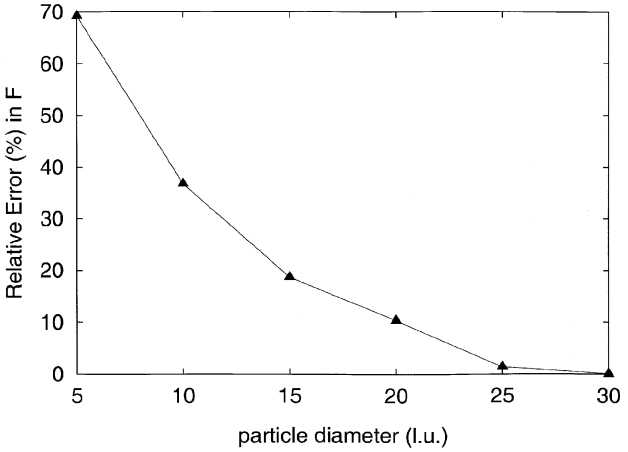

Figure 1. Finite-size simulations: relative error (in %) based on the $2a = 30$ case, in the drag force computed on different grid resolutions.

In all simulations, the positions of the particles are the same. The volume fraction of the system is 0.62 (worst-case scenario). The relaxation parameter $\tau = 1.0$.

calibration procedure, the results obtained by using radii of 10 ($\phi = 0.29$) and 20 lattice points ($\phi = 0.274$), respectively, match satisfactorily well. Some differences may be expected due to a mismatch in the exact value of ϕ.

Apart from the issues related to resolution sensitivity, the computed drag forces suffer from statistical fluctuations due to heterogeneities associated with the arrangements of the spheres. These effects can be reduced by averaging the results obtained by a series of simulations with different geometrical configurations. The mean drag-force is defined as the ensemble average of the drag forces obtained by n_c independent simulations

$$\langle F \rangle = \frac{1}{n_c} \sum_{i=1}^{n} F_i$$

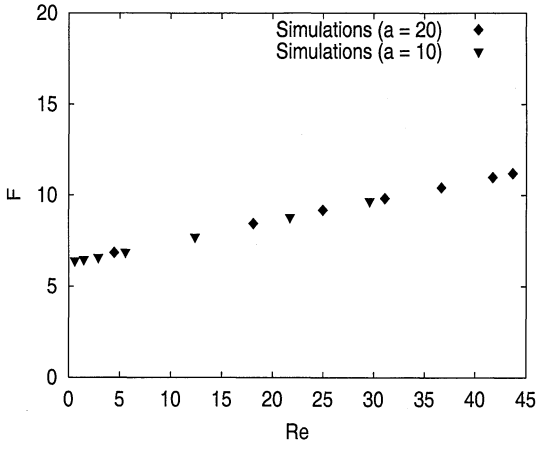

Figure 2. Finite-size simulations: calibration of the simulation results by the hydrodynamic radius.

The volume fraction of the packed bed is 0.29 (for $a = 10$) and 0.274 (for $a = 20$). The relaxation parameter $\tau = 0.7$.

Analogous to the work of Hill et al. (2001), the uncertainty in the estimated mean is computed from

$$\Delta F = \sqrt{\frac{\mathrm{var}(F)}{n_c - 1}}$$

with $\mathrm{var}(F) = \langle (F - \langle F \rangle)^2 \rangle$ denoting the variance of F (see Hill et al., 2001, and references therein).

The geometrical configuration of the spheres is generated by the method described in (Kandhai et al. (2002a). Note that in the extreme case of "closed" packed systems, the structure of the medium used in the computations might be different as compared to that of the packed beds used in the experimental measurements.

It should be noted that in the simulations considered here, the particle positions are held fixed. As discussed in the first section, in two-fluid models, the macroscopic equations are derived based on some averaging principle. The presence of a certain amount of solid phase is then modeled by the solid volume fraction parameter, ϵ_s. Furthermore, there is no direct characterization of the geometrical stucture of the solid particles. Therefore, drag relations obtained from ensemble averaging of the systems considered here are useful as closure relations in the two-fluid models. Apart from that, in gas–solid flows, the response time of the particle dynamics due to disturbances in the flow ($\tau_p = ((\rho_p/\rho_f)(d_p^2/18\nu))$, is very large—on the order of 1,000—compared to the time-scale related to hydrodynamic disturbances in fluid ($\tau_c = d_p/U_s$). It is, therefore, expected that the ensemble-averaged behavior of systems with fixed particles may be similar to that of homogeneous fluidized systems in the equilibrium state. In Figure 3, we show the average slip velocity as a function of

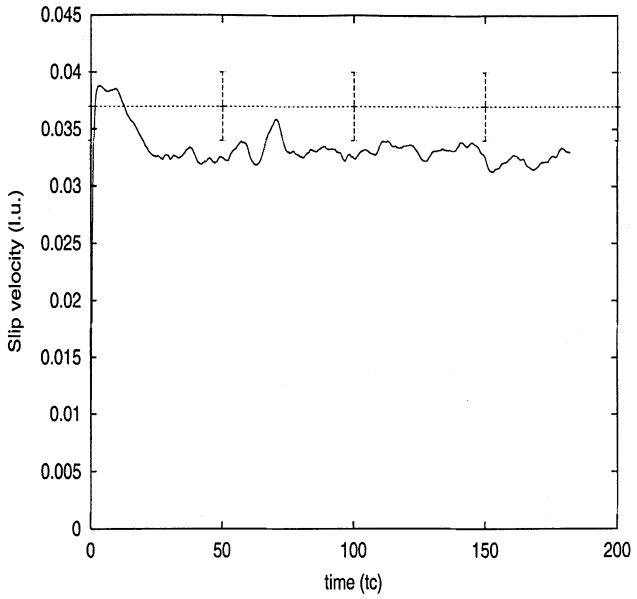

Figure 3. Transient behavior of the drag force for a system of freely moving particles compared to the average drag force obtained for a fixed array of particles; the dimension of the simulation domain is $8a \times 8a \times 8a$, $\phi = 0.27$, $a = 10$, $Re \approx 10$, and $\rho_p/\rho_f = 1{,}000$.

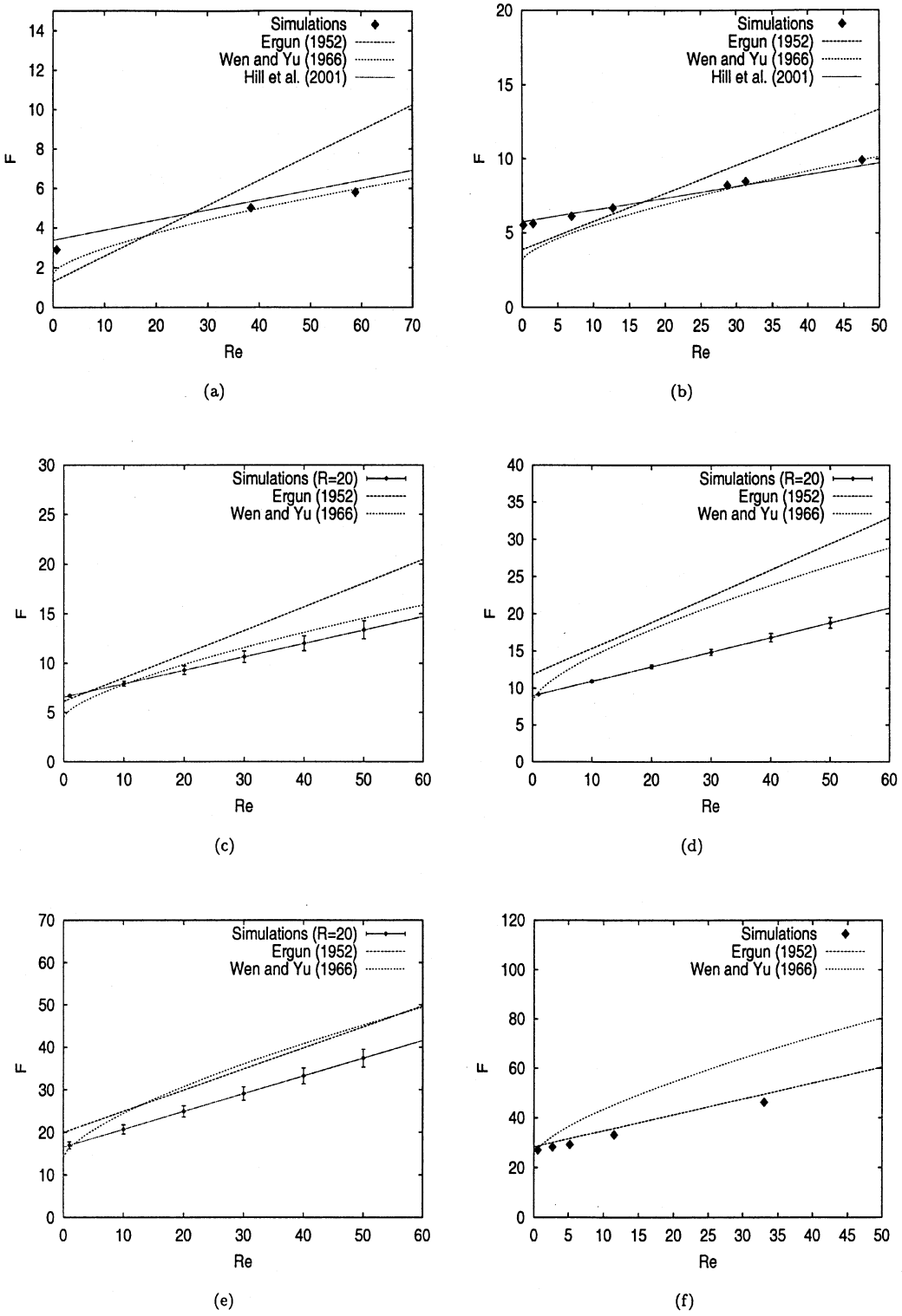

Figure 4. Drag force as a function of *Re* for a disordered periodic array of spheres with varying solid volume fractions $\phi = 0.1$ to 0.5.

The exact values of the volume fractions are: from (a) to (f) $\phi = 0.10, 0.19, 0.27, 0.36, 0.43$, and 0.48. The Ergun and Wen and Yu equations are included in all graphs. Furthermore the results obtained by Hill are also shown for the volume-fractions with a close match. The dimensions of the simulation domain are $8a \times 8a \times 8a$, with a the radius of the spheres in lattice units (l.u.), $a = 10$ for $\phi < 0.3$ and $a = 20$ for $\phi > 0.3$. The number of spheres is varied from 16 to 64.

the time of systems of freely moving particles (with $\phi = 0.27$, $a = 10$, $Re \approx 10$, and $\rho_p/\rho_f = 1{,}000$) and compare that with the averaged ensemble slip velocity of systems with particle positions fixed. It is evident that the average slip velocity of the dynamic system is close to that of the "fixed" system, when we take into account variations due to the uncertainty in the estimated mean. Similar results have been obtained for other volume fractions ($\phi \approx 0.1$ and $\phi \approx 0.2$, respectively). Notice that the structure of fixed and sedimenting systems might be different, especially in the case of liquid–solid suspensions.

The eventual simulations were carried out for periodic boxes with dimension of $8a \times 8a \times 8a$, the corresponding grid dimensions being $80 \times 80 \times 80$ (for $\phi < 0.3$) and $160 \times 160 \times 160$ (for $\phi > 0.3$), respectively. The memory requirements for these simulations were at most 600 Mb, and the number of time steps to reach steady state was varied from 10,000 to 2,000 time steps for increasing solid-volume fraction.

We now return to our main question, whether the Wen and Yu and the Ergun correlations do capture the complete range of solid-volume fractions. Figure 4 shows, the results for the dimensionless drag force as a function of the Reynolds number for increasing solid-volume fraction. The corresponding curves of the Wen and Yu and the Ergun correlations are included in all plots. Moreover, in Figure 4a and 4b, we also have included the results obtained by Hill et al. (2001). These are the only two cases in which there is a close match in the solid-volume fractions considered in both studies. We clearly see that there is a good agreement between both simulations. This point is further confirmed in Figures 5 and 6. Figures 5 and 6 show the slope of F vs. Re as a function of ϕ, and the functional dependence of F on ϕ as a function of the void fraction, respectively.

As discussed earlier, an eventual transition region is expected to occur in the range of solid-volume fractions between 0.2 and 0.4. Therefore, we spend most of our computational effort in this specific range: the mean drag force and the uncertainty in the estimated mean were computed using the method described earlier with $n_c = 10$. For the other volume fractions, we restricted the computations to a single geometrical configuration, in order to reduce the total computation time. Before discussing the final results, we still would like to address a subtle point. As mentioned in the previous section, the flow in the simulations was driven by a body force. Consequently, the average velocity could not be predicted in advance, but was dependent on the geometrical configuration. For each geometrical configuration, however, we found that a linear relation fits all the simulated points very well (with errors in the fitting parameters $\leq 0.5\%$). Therefore, we used the fitted expressions to estimate the drag force for specific values of Re and then computed the mean based on these values.

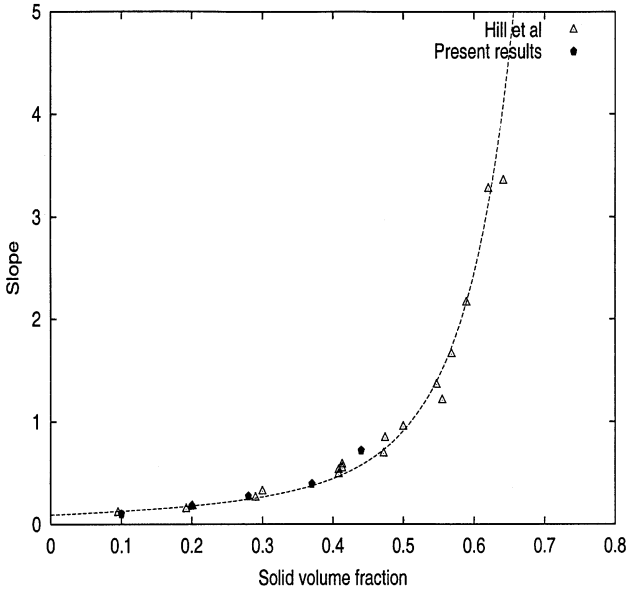

Figure 5. Slope of F vs. Re as a function of ϕ; the solid line is the fit expression obtained by Hill et al. (2001).

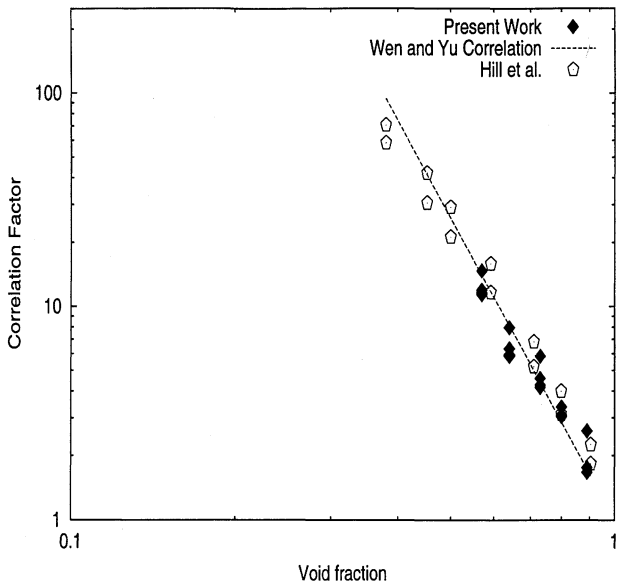

Figure 6. Functional dependence of F on ϕ as a function of the void fraction.

The solid line is the Wen and Yu (1966) correlation.

The first observation in Figure 4 is that our results are indeed in good agreement with the Wen and Yu correlation for the low solid-volume fractions and the Ergun correlation for the high solid-volume fractions. The interesting feature is that the Wen and Yu correlation shows a better match with the simulation results, even for $\phi \approx 0.3$. The Ergun equation is found to be valid for $\phi \approx 0.5$. It is evident that for $0.3 \leq \phi \leq 0.43$ both the Wen and Yu and the Ergun correlation show a discrepancy with the computed values, which suggests that there is indeed an intermediate regime. If uncertainties on the order of 10% are acceptable, the fit-correlation obtained by Hill et al., and found to be consistent with our results, can be used as a closure relation for $0 < Re < 100$. However, to provide an even more accurate correlation for the intermediate regime, more detailed simulations based on finer grid resolutions or by using more sophisticated methods for imposing no-slip boundary conditions in lattice–Boltzmann simulations (Rohde et al., 2002), are still necessary.

Acknowledgments

The work is part of the research program of the Dutch Research School on Process Technology, "Onderzoekschool Proces Technologie (OSPT)." It is financially supported by Akzo-Nobel, DSM and Shell Research. We thank Prof. Dr. Ir. J. A. M. Kuipers, (Universiteit Twente) for many useful discussions.

Literature Cited

Chen, S., and G. D. Doolen, "Lattice Boltzmann Method for Fluid Flows," *Annu. Rev. Fluid Mech.*, **30**, 329 (1998).

Derksen, J. J., and H. E. A. Van den Akker, "Large Eddy Simulations on the Flow Driven in a Rushton Turbine," *AIChE J.*, **45**, 209 (1999).

Ergun, S., "Fluid Flow Through Packed Columns," *Chem. Eng. Prog.*, **48**, 245 (1952).

Fan L. S., and C. Zhu, *Principles of Gas-Solid Flows*, Cambridge Univ. Press, Cambridge (1998).

Geldart, D., *Gas Fluidization Technology*, Wiley, New York (1986).

Gidaspow, D., *Multiphase Flow and Fluidization*, Academic Press, San Diego (1994).

Goldschmidt, M. J. V., B. P. B. Hoomans, and J. A. M. Kuipers, "Recent Progress Towards Hydrodynamic Modeling of Dense Gas-Particle Flows," *Recent Res. Dev. Chem. Eng.*, **4**, 273 (2000).

Hasimoto, H., "On the Periodic Fundamental Solutions of the Stokes Equations and Their Application to Viscous Flow Past a Cubic Array of Spheres," *J. Fluid Mech.*, **5**, 317 (1959).

Hill, R. J., D. L. Koch, and A. J. C. Ladd, "Moderate-Reynolds-Number Flows in Ordered and Random Arrays of Spheres," *J. Fluid Mech.*, **448**, 243 (2001).

Kandhai, D., A. Koponen, A. Hoekstra, M. Kataja, J. Timonen, and P. M. A. Sloot, "Implementation Aspects of 3D Lattice-BGK: Boundaries, Accuracy and a New Fast Relaxation Method," *J. Comput. Phys.*, **150**, 482 (1999).

Kandhai, D., U. Tallarek, D. Hlushkou, A. G. Hoekstra, P. M. A. Sloot, and H. van As, "Numerical Simulation and Measurement of Liquid Holdup in Biporous Media Containing Discrete Stagnant Zones," *Philos. Trans. R. Soc. London A*, **360**, 521 (2002a).

Kandhai, D., D. Hlushkou, A. G. Hoekstra, P. M. A. Sloot, H. van As, and U. Tallarek, "Influence of Stagnant Zones on Transient and Asymptotic Dispersion in Macroscopically Homogeneous Porous Media," *Phys. Rev. Lett.*, **88**, 234501 (2002b).

Koch, D. L., "Kinetic Theory for a Monodisperse Gas-Solid Suspension," *Phys. Fluids A*, **2**, 1711 (1990).

Ladd, A. J. C., "Numerical Simulations of Particulate Suspensions Via a Discretized Boltzmann Equation. Part 2. Numerical Results," *J. Fluid Mech.*, **271**, 311 (1994).

Richardson, J. F., and W. N. Zaki, "Sedimentation and Fluidization: Part I," *Trans. Inst. Chem. Eng.*, **32**, 35 (1954).

Rohde, M., J. J. Derksen, and H. E. A. Van den Akker, "Volumetric Method for Calculating the Flow Around Moving Objects in Lattice-Boltzmann Schemes," *Phys. Rev. E*, **65**, 056701 (2002).

Van Wachem, B. G. M., J. C. Schouten, C. M. van den Bleek, R. Krishna, and J. L. Sinclair, "Comparative Analysis of CFD Models of Dense Gas-Solid Systems," *AIChE J.*, **47**, 1035 (2001).

Wen, Y. C., and Y. H. Yu, "Mechanics of Fluidization," *Chem. Eng. Prog. Symp. Ser.*, **62**, 100 (1966).

Manuscript received Feb. 14, 2002, and revision received Sept. 18, 2002.